



On the Mass Accretion Rate and Infrared Excess in Herbig Ae/Be Stars

R. Arun¹ , Blesson Mathew¹ , P. Manoj² , K. Ujjwal¹, Sreeja S. Kartha¹, Gayathri Viswanath¹, Mayank Narang² , and K. T. Paul¹

¹ Department of Physics and Electronics, CHRIST (Deemed to be University), Bangalore 560029, India; blesson.mathew@christuniversity.in

² Department of Astronomy and Astrophysics, Tata Institute of Fundamental Research, Homi Bhabha Road, Colaba, Mumbai 400005, India

Received 2019 February 11; revised 2019 February 28; accepted 2019 March 1; published 2019 April 2

Abstract

The present study makes use of the unprecedented capability of the *Gaia* mission to obtain the stellar parameters such as distance, age, and mass of HAeBe stars. The accuracy of *Gaia* DR2 astrometry is demonstrated from the comparison of the *Gaia* DR2 distances of 131 HAeBe stars with the previously estimated values from the literature. This is one of the initial studies to estimate the age and mass of a confirmed sample of HAeBe stars using both the photometry and distance from the *Gaia* mission. Mass accretion rates are calculated from H α line flux measurements of 106 HAeBe stars. Since we used distances and the stellar masses derived from the *Gaia* DR2 data in the calculation of the mass accretion rate, our estimates are more accurate than previous studies. The mass accretion rate is found to decay exponentially with age, from which we estimated a disk dissipation timescale of 1.9 ± 0.1 Myr. The mass accretion rate and stellar mass exhibit a power-law relation of the form $\dot{M}_{\text{acc}} \propto M_*^{2.8 \pm 0.2}$. From the distinct distribution in the values of the infrared spectral index, $n_{2-4.6}$, we suggest the possibility of difference in the disk structure between Herbig Be and Herbig Ae stars.

Key words: accretion, accretion disks – protoplanetary disks – stars: emission-line, Be – stars: pre-main sequence – stars: variables: T Tauri, Herbig Ae/Be

Supporting material: machine-readable table

1. Introduction

Herbig Ae/Be stars are intermediate-mass pre-main sequence (PMS) stars with masses between 2 and 10 M_{\odot} . They are often used to understand the missing link in the star formation sequence connecting T Tauri stars and massive young stellar objects (YSOs; e.g., Herbig 1960; Waters & Waelkens 1998; Oudmaijer et al. 2017). Herbig Ae/Be stars (hereafter HAeBe) show emission lines in their spectrum and exhibit infrared excess (known as IR excess) in the continuum, suggestive of hot and/or cool dust in the circumstellar medium (CSM; Hillenbrand et al. 1992; Malfait et al. 1998). The emission lines such as H α are formed in the CSM and are used for understanding the mass accretion process in HAeBe stars (e.g., Hamann & Persson 1992; Vieira et al. 2003; Manoj et al. 2006; Mendigutía et al. 2011a, 2011b).

Understanding the accretion of material from the CSM is important to study the PMS evolution because it can provide vital information about the formation and evolution of planets around the stars (Muzerolle et al. 2003; Beltrán and de Wit 2016). It is proposed that Herbig Ae (HAe) and Herbig Be (HBe) stars may show considerable differences in disk morphology and mode of accretion (Vink et al. 2002; Alonso-Albi et al. 2009; Vioque et al. 2018). However, in order to establish these results, we need to have precise distance measurements. This is due to the fact that the precision of stellar parameters such as age, mass, $\log(g)$, etc., strongly depend on precise distance measurements. One of the pioneering missions that provided accurate distances of nearby astronomical objects was the *Hipparcos* mission. Based on the distance measurements of nearby HAeBe stars from the *Hipparcos* mission (ESA 1997), van den Ancker et al. (1998) derived the astrophysical parameters of a sample of 44 HAeBe stars and found that 65% of HAeBe stars show photometric variability. It may be noted that *Hipparcos* provided reliable

distance values for stars within 1 kpc to the Sun (de Zeeuw et al. 1999). The *Gaia* mission is designed to provide high-quality astrometry and photometry of 1.3 billion stars (Gaia Collaboration et al. 2016a, 2016b). With the second data release of *Gaia* (*Gaia* DR2), it is possible to get parallax measurements of stars with uncertainties limited to 0.04 mas, for sources brighter than $G = 14$ mag (Gaia Collaboration et al. 2018b; Luri et al. 2018). From precise distance measurements, it is possible to derive the relations connecting the IR excess and mass accretion rates (\dot{M}_{acc}) with the stellar parameters of HAeBe stars. This can be used to understand whether magnetospheric or disk accretion plays a major role in HAeBe stars.

In this work, we estimate the stellar parameters of a well-studied sample of HAeBe stars, thereby understanding the mass accretion process in PMS stars. We present the sample of HAeBe stars used for this study in Section 2. The results of this study are presented in Section 3, wherein we discuss the procedure associated with distance and extinction measurements. Also, we estimate the mass and age of HAeBe stars and discuss mass accretion in HAeBe stars. Recently, Vioque et al. (2018) estimated the stellar parameters of HAeBe stars using distance measurements from the *Gaia* DR2. They based their analysis on the derived quantities such as luminosity and temperature, which can introduce additional errors in the estimation of the mass and age of HAeBe stars. Instead, in the present study, we based the analysis on the *Gaia* color-magnitude diagram (CMD). The main results are summarized in Section 4.

2. Data Inventory

A sample of 142 stars is taken from Mathew et al. (2018), which is a carefully selected, well-studied sample of HAeBe stars from The et al. (1994), Manoj et al. (2006), and Fairlamb et al. (2015).

Mathew et al. (2018) discussed various mechanisms for the formation of OI emission lines in HAeBe stars and found that Lyman beta fluorescence is the dominant excitation mechanism. This is the second work in the series studying the \dot{M}_{acc} and IR excess in HAeBe stars. Here we re-estimate the relations connecting the \dot{M}_{acc} with the stellar parameters such as age and mass in the context of the *Gaia* DR2 release. These new estimates will be used for our future work to explore the possibility of using the OI 8446 Å emission line as an accretion indicator in HAeBe stars (B. Mathew et al. 2019, in preparation).

The coordinates, proper motions, and V magnitudes of the 142 stars are taken from the literature. R.A. and decl. of these stars are converted from J2000 to J2015.5 epoch using their proper motion. A query for a *Gaia* DR2 match for these stars was then performed around the converted coordinates with a search radius of 10 arcsec via the Mikulski Archive for Space Telescopes.³ If a match was not found, then the search radius was increased up to 30 arcsec. This procedure returned 354 *Gaia* DR2 rows for 142 stars. For 60 stars, only one *Gaia* DR2 match was returned. For the remaining 82 stars with multiple entries, those which had $|G - V| \text{ mag} > 3.5$ were removed. For the remaining multiple entries, the *Gaia* DR2 row with the closest positional match was selected for which $|G - V| \text{ mag} \leq 2$. Thus we got the *Gaia* DR2 parallax and magnitudes for all stars in the sample. After avoiding 11 sources, where 6 showed no parallax data and 5 had negative parallax, we finalized our sample of HAeBe stars to be 131. These stars are found in the distance range of 0.09–6 kpc, with a range in *Gaia* G -band magnitude from 4.4 to 14.5 mag.

3. Results

3.1. Comparison of the *Gaia* DR2 Distances with Previous Estimates

The uncertainty in the distance determination of stars is mitigated to a considerable extent due to the precision of the *Gaia* mission. Although *Gaia* DR2 provides accurate positions and parallax measurements via a rigorous astrometric reduction technique, the estimation of distance by simple inversion of the *Gaia* parallax does entail certain inherent problems. The distance obtained through such a method is acceptable only when the parallax measurements are fairly precise, i.e., when the signal-to-noise ratio (S/N) of the parallax measurement is preferably high ($S/N \geq 5$). In cases where fractional parallax uncertainty is high, the probability distribution for the distance inferred from the inverted parallax becomes strongly asymmetric and non-Gaussian in nature. Furthermore, the distance thus estimated will be nonphysical if the concerned parallax measurement is negative, owing to the large measurement noise or due to the star moving opposite to the direction of the true parallactic motion. To tackle this problem, Bailer-Jones et al. (2018) applied a probabilistic approach to estimate distances to 1.3 billion stars having *Gaia* DR2 data. They adopted the distance likelihood (inferred from the *Gaia* parallax) and a distance prior (an exponentially decreasing space density prior that is based on a Galaxy model) approach. The distance estimates and corresponding uncertainties thus determined are purely geometric and devoid of any underlying assumptions. Hence, for the present study, we use the distance estimates from Bailer-Jones et al. (2018), which are listed in Table 1.

We compared the distance estimated from the *Gaia* DR2 with the values listed in the literature. Manoj et al. (2006) compiled the distances of HAeBe stars from various studies and provided the best estimate of the distance for each star. This is supplemented with the distance information from the *Gaia* DR1 (Gaia Collaboration et al. 2016b) and those given in Fairlamb et al. (2015). The extreme values of distance from these compilations are included in Figure 1 along with the *Gaia* DR2 estimates. It can be seen from the figure that the distance estimate from the *Gaia* DR2 is more accurate (with minimal error) than previous estimates.

3.2. Extinction Calculation

The extinction in all of the photometric bands, G , G_{BP} , and G_{RP} , are listed in the *Gaia* archive. But this extinction and reddening values are limited to a small number of objects. The extinction calculation is done by an automated algorithm, which is explained in detail in Evans et al. (2018). Also, they have listed the caveats involved in the automated way of estimating extinction values. For this work, we have independently estimated the extinction values from the extinction curve of McClure (2009). From the curve we calculated $\left[\frac{A_G}{A_V}\right]$, $\left[\frac{A_{G_{\text{BP}}}}{A_V}\right]$, and $\left[\frac{A_{G_{\text{RP}}}}{A_V}\right]$.

The A_V values for our sample of HAeBe stars are taken from Fairlamb et al. (2015), Chen et al. (2016), and Mathew et al. (2018). Hernández et al. (2004) suggested using high values of total-to-selective extinction ($R_V = 5$) for estimating the extinction values of HAeBe stars. This is suggestive of the grain growth in the disk of HAeBe stars (Gorti & Bhatt 1993; Manoj et al. 2006). For the present work, we adopted $R_V = 5$ while calculating the extinction (A_V) values. This method was followed while calculating the A_V values of HAeBe stars in Mathew et al. (2018). Hence, for this analysis, we included the A_V values of HAeBe stars that are listed in Mathew et al. (2018). For the remaining stars, A_V values are taken from Fairlamb et al. (2015) and Chen et al. (2016), which are re-estimated for $R_V = 5$. It may be noted that Hernández et al. (2004) pointed out that the age and luminosity of HAeBe stars better match with those of PMS stars when $R_V = 5$ is employed. The A_V values estimated for all of the HAeBe stars will be used to correct the *Gaia* photometry for extinction.

The mean wavelength values in the *Gaia* passbands and Johnson V band are taken from Jordi et al. (2010). The $\left[\frac{A_G}{A_V}\right]$, $\left[\frac{A_{G_{\text{BP}}}}{A_V}\right]$, and $\left[\frac{A_{G_{\text{RP}}}}{A_V}\right]$ values for different ranges of A_V are calculated using McClure (2009), which are listed below.

For $A_V \leq 2.5$

$$\frac{A_G}{A_V} = 0.831, \quad \frac{A_{G_{\text{BP}}}}{A_V} = 1.032, \quad \frac{A_{G_{\text{RP}}}}{A_V} = 0.678. \quad (1)$$

For $2.5 < A_V < 7.5$

$$\frac{A_G}{A_V} = 0.831, \quad \frac{A_{G_{\text{BP}}}}{A_V} = 1.028, \quad \frac{A_{G_{\text{RP}}}}{A_V} = 0.672. \quad (2)$$

For $7.5 \leq A_V$

$$\frac{A_G}{A_V} = 0.831, \quad \frac{A_{G_{\text{BP}}}}{A_V} = 1.028, \quad \frac{A_{G_{\text{RP}}}}{A_V} = 0.672. \quad (3)$$

³ <https://archive.stsci.edu/>

Table 1
Stellar Parameters for Our Sample of 131 HAcBe Stars

Object	Distance (pc)	Age (Myr)	V18 Age (Myr)	Mass (M_{\odot})	V18 Mass (M_{\odot})
51 Oph	123 $^{+5}_{-4}$	1.02 $^{+0.02}_{-0.02}$	1.22 $^{+0.29}_{-0.57}$	4 $^{+0.03}_{-0.02}$	3.35 $^{+0.79}_{-0.22}$
AB Aur	162 $^{+2}_{-2}$	3.92 $^{+0.02}_{-0.01}$	4 $^{+1.4}_{-1.5}$	2.34 $^{+0.01}_{-0.01}$	2.15 $^{+0.36}_{-0.21}$
AK Sco	140 $^{+1}_{-1}$	6.94 $^{+2.91}_{-2.41}$	8.4 $^{+1.7}_{-0.4}$	1.62 $^{+0.19}_{-0.17}$	1.401 $^{+0.07}_{-0.07}$
AS 220	220 $^{+7}_{-7}$...	18.5 $^{+1.5}_{-1.4}$...	1.513 $^{+0.076}_{-0.076}$ ^a
AS 442	843 $^{+22}_{-21}$	0.26 $^{+0.02}_{-0.02}$	0.84 $^{+0.19}_{-0.19}$	6.9 $^{+0.22}_{-0.2}$	3.89 $^{+0.35}_{-0.26}$
AS 443	826 $^{+20}_{-19}$	0.13 $^{+0.01}_{-0.01}$	1.13 $^{+0.91}_{-0.37}$	11.2 $^{+0.1}_{-0.09}$	3.5 $^{+0.48}_{-0.64}$
AS 505	855 $^{+23}_{-21}$	0.28 $^{+0.01}_{-0.01}$	0.188 $^{+0.095}_{-0.065}$ ^a	5.8 $^{+0.02}_{-0.02}$	6.8 $^{+1}_{-0.9}$
BD+40 4124	893 $^{+26}_{-24}$	<0.1	0.1 $^{+0.11}_{-0.07}$	10.77 $^{+0.14}_{-0.14}$	9.1 $^{+3.9}_{-1.8}$
BD+46 3471	759 $^{+17}_{-16}$	0.86 $^{+0.01}_{-0.01}$	1.25 $^{+0.64}_{-0.73}$	4.2 $^{+0.02}_{-0.01}$	3.3 $^{+1.1}_{-0.4}$
BD+61 154	561 $^{+9}_{-9}$	0.17 $^{+0.01}_{-0.01}$	1.89 $^{+0.49}_{-0.78}$	9.5 $^{+0.27}_{-0.17}$	2.94 $^{+0.59}_{-0.23}$
BD+65 1637	874 $^{+20}_{-19}$	0.3 $^{+0.01}_{-0.01}$	0.41 $^{+0.15}_{-0.13}$	6.42 $^{+0.02}_{-0.02}$	5.31 $^{+0.69}_{-0.48}$
BF Ori	385 $^{+8}_{-8}$	5.08 $^{+0.38}_{-0.36}$	6.38 $^{+0.32}_{-0.46}$	2.11 $^{+0.35}_{-0.03}$	1.807 $^{+0.09}_{-0.09}$
BH Cep	371 $^{+3}_{-3}$	12.73 $^{+0.21}_{-0.21}$	10.6 $^{+3}_{-3.1}$	1.57 $^{+0.01}_{-0.01}$	1.37 $^{+0.15}_{-0.1}$
BO Cep	332 $^{+2}_{-2}$	8.66 $^{+1.88}_{-0.43}$	17.1 $^{+0.9}_{-2.4}$	1.49 $^{+0.07}_{-0.05}$	1.215 $^{+0.061}_{-0.061}$ ^a
CD-42 11721	1634 $^{+164}_{-137}$	<0.1	0.023 $^{+0.026}_{-0.012}$ ^a	10.38 $^{+0.13}_{-0.13}$	20 $^{+7}_{-5}$
CPD-61 3587B	2672 $^{+303}_{-248}$	<0.1	...	13.3 $^{+0.2}_{-0.5}$...
CQ Tau	162 $^{+2}_{-2}$	10.82 $^{+2.49}_{-1.87}$	8.9 $^{+2.8}_{-2.5}$	1.65 $^{+0.05}_{-0.15}$	1.47 $^{+0.19}_{-0.11}$
DG Cir	821 $^{+30}_{-28}$	0.25 $^{+0.06}_{-0.06}$	4 $^{+16}_{-3}$	6.94 $^{+1.12}_{-0.68}$	2.3 $^{+0.6}_{-0.65}$
DX Cha	108 $^{+1}_{-1}$	3.52 $^{+0.02}_{-1.02}$	5.48 $^{+0.27}_{-0.41}$	2.48 $^{+0.01}_{-0.01}$	1.849 $^{+0.092}_{-0.092}$ ^a
HBC 334	1774 $^{+109}_{-98}$	2.32 $^{+0.05}_{-0.05}$	3.71 $^{+0.49}_{-0.19}$	2.94 $^{+0.02}_{-0.03}$	2.1 $^{+4.3}_{-1.1}$
HD 100453	104 $^{+0}_{-0}$	12.88 $^{+0.02}_{-0.03}$	6.53 $^{+0.45}_{-0.49}$	1.61 $^{+0.01}_{-0.01}$	1.251 $^{+0.063}_{-0.063}$ ^a
HD 100546	110 $^{+1}_{-1}$	5.08 $^{+0.06}_{-0.08}$	5.5 $^{+1.4}_{-0.8}$	2.49 $^{+0.02}_{-0.02}$	2.05 $^{+0.1}_{-0.12}$
HD 101412	407 $^{+5}_{-5}$	3.48 $^{+0.02}_{-0.02}$	4.37 $^{+0.22}_{-0.32}$	2.51 $^{+0.08}_{-0.01}$	2.1 $^{+0.11}_{-0.11}$
HD 114981	699 $^{+32}_{-29}$	0.23 $^{+0.01}_{-0.01}$	0.277 $^{+0.053}_{-0.068}$ ^a	7.07 $^{+0.07}_{-0.07}$	6.09 $^{+0.59}_{-0.34}$
HD 130437	1662 $^{+107}_{-95}$	<0.1	0.046 $^{+0.077}_{-0.026}$ ^a	20.45 $^{+0.21}_{-0.2}$	13.4 $^{+4.6}_{-3.8}$
HD 132947	378 $^{+8}_{-8}$...	4.05 $^{+0.32}_{-0.2}$...	2.22 $^{+0.11}_{-0.11}$
HD 135344B	135 $^{+1}_{-1}$	8.93 $^{+0.04}_{-0.03}$	8.93 $^{+0.45}_{-0.91}$	1.52 $^{+0.01}_{-0.01}$	1.432 $^{+0.072}_{-0.072}$ ^a
HD 139614	134 $^{+1}_{-1}$	14.1 $^{+0.03}_{-0.03}$	14.5 $^{+1.4}_{-3.6}$	2.35 $^{+0.01}_{-0.01}$	1.481 $^{+0.074}_{-0.074}$ ^a
HD 141569	110 $^{+1}_{-1}$	7.2 $^{+0.02}_{-0.02}$	9 $^{+11}_{-1}$	2.14 $^{+0.01}_{-0.01}$	1.86 $^{+0.093}_{-0.093}$ ^a
HD 141926	1345 $^{+88}_{-78}$	<0.1	0.023 $^{+0.007}_{-0.005}$ ^a	>25	19.5 $^{+2.4}_{-2.2}$
HD 142527	157 $^{+1}_{-1}$	2.96 $^{+0.02}_{-0.02}$	6.6 $^{+0.3}_{-1.5}$	2.4 $^{+0.01}_{-0.01}$	1.61 $^{+0.12}_{-0.08}$
HD 142666	148 $^{+1}_{-1}$	7.27 $^{+0.08}_{-0.07}$	9.33 $^{+0.77}_{-0.47}$	1.82 $^{+0.01}_{-0.01}$	1.493 $^{+0.075}_{-0.075}$ ^a
HD 144432	155 $^{+1}_{-1}$	7.24 $^{+0.02}_{-0.02}$	4.98 $^{+0.25}_{-0.55}$	1.81 $^{+0.01}_{-0.01}$	1.386 $^{+0.069}_{-0.069}$ ^a
HD 145718	152 $^{+2}_{-2}$	5.7 $^{+0.17}_{-0.13}$	9.8 $^{+2.8}_{-0.5}$	2.09 $^{+0.17}_{-0.04}$	1.605 $^{+0.08}_{-0.08}$
HD 150193A	150 $^{+2}_{-2}$	4.55 $^{+0.03}_{-0.03}$	5.48 $^{+0.44}_{-0.27}$	2.2 $^{+0.01}_{-0.01}$	1.891 $^{+0.095}_{-0.095}$ ^a
HD 163296	101 $^{+1}_{-1}$	6.52 $^{+0.26}_{-0.25}$	7.6 $^{+1.1}_{-1.2}$	2.1 $^{+0.02}_{-0.02}$	1.833 $^{+0.092}_{-0.092}$ ^a
HD 179218	264 $^{+3}_{-3}$	2.24 $^{+0.01}_{-0.01}$	1.66 $^{+0.54}_{-0.26}$	2.95 $^{+0.01}_{-0.01}$	2.98 $^{+0.18}_{-0.3}$
HD 190073	872 $^{+55}_{-49}$	0.26 $^{+0.01}_{-0.01}$	0.22 $^{+0.11}_{-0.07}$	5.99 $^{+0.06}_{-0.05}$	5.89 $^{+0.8}_{-0.76}$
HD 200775	357 $^{+6}_{-6}$	0.11 $^{+0.01}_{-0.01}$	0.41 $^{+0.15}_{-0.2}$	9.41 $^{+0.07}_{-0.06}$	5.3 $^{+1.3}_{-0.5}$
HD 216629	790 $^{+18}_{-17}$	0.11 $^{+0.01}_{-0.01}$	0.07 $^{+0.044}_{-0.033}$ ^a	8.22 $^{+0.02}_{-0.02}$	9.8 $^{+2.7}_{-1.3}$
HD 244314	427 $^{+11}_{-11}$	7.93 $^{+0.05}_{-0.06}$	7.43 $^{+0.37}_{-0.54}$	1.77 $^{+0.01}_{-0.01}$	1.691 $^{+0.093}_{-0.085}$ ^a
HD 244604	417 $^{+11}_{-11}$...	4.89 $^{+0.24}_{-0.52}$...	1.98 $^{+0.1}_{-0.1}$
HD 245185	427 $^{+21}_{-19}$	5.54 $^{+0.22}_{-0.14}$	8 $^{+12}_{-3}$	2.2 $^{+0.01}_{-0.01}$	1.92 $^{+0.18}_{-0.1}$
HD 250550	704 $^{+54}_{-47}$	1.7 $^{+0.05}_{-0.05}$	2.56 $^{+0.43}_{-0.67}$	3.26 $^{+0.04}_{-0.03}$	2.6 $^{+0.3}_{-0.14}$
HD 259431	712 $^{+25}_{-23}$	0.25 $^{+0.01}_{-0.01}$	0.42 $^{+0.53}_{-0.28}$	6.28 $^{+0.04}_{-0.02}$	5.2 $^{+1.8}_{-1.3}$
HD 287823	356 $^{+7}_{-7}$	6.04 $^{+0.05}_{-0.05}$	7.43 $^{+0.37}_{-0.37}$	2.27 $^{+0.01}_{-0.01}$	1.704 $^{+0.085}_{-0.085}$ ^a
HD 290409	451 $^{+17}_{-16}$...	7 $^{+13}_{-2}$...	1.9 $^{+0.18}_{-0.09}$
HD 290500	434 $^{+13}_{-13}$	8.36 $^{+0.17}_{-0.09}$	10.4 $^{+9.3}_{-3.3}$	2.04 $^{+0.05}_{-0.05}$	1.383 $^{+0.082}_{-0.069}$ ^a
HD 290764	394 $^{+10}_{-10}$	6.4 $^{+0.06}_{-0.05}$	6.9 $^{+0.5}_{-1.4}$	1.88 $^{+0.01}_{-0.01}$	1.69 $^{+0.13}_{-0.08}$
HD 290770	396 $^{+12}_{-11}$	4.3 $^{+0.11}_{-0.09}$	4.59 $^{+0.49}_{-0.54}$	2.39 $^{+0.02}_{-0.02}$	2.22 $^{+0.11}_{-0.11}$
HD 305298	5905 $^{+1119}_{-829}$	<0.1	0.04 $^{+0.31}_{-0.01}$	17.76 $^{+0.46}_{-0.48}$	17.7 $^{+2.1}_{-2}$
HD 31648	161 $^{+2}_{-2}$	5.65 $^{+0.02}_{-0.02}$	6.2 $^{+0.3}_{-1.1}$	2.06 $^{+0.01}_{-0.01}$	1.78 $^{+0.13}_{-0.09}$
HD 35187	162 $^{+3}_{-3}$	5.99 $^{+0.25}_{-0.94}$	5 $^{+5}_{-2}$	2.02 $^{+0.32}_{-0.12}$	2.1 $^{+0.25}_{-0.25}$
HD 35929	384 $^{+8}_{-8}$	1.16 $^{+0.01}_{-0.01}$	1.46 $^{+0.07}_{-0.17}$	3.48 $^{+0.01}_{-0.01}$	2.92 $^{+0.15}_{-0.15}$
HD 36112	160 $^{+2}_{-2}$	8 $^{+0.03}_{-0.04}$	8.3 $^{+0.4}_{-1.4}$	1.78 $^{+0.01}_{-0.01}$	1.56 $^{+0.11}_{-0.08}$
HD 37258	360 $^{+13}_{-13}$	7.1 $^{+0.62}_{-0.03}$	8 $^{+12}_{-2}$	1.93 $^{+0.05}_{-0.1}$	1.88 $^{+0.14}_{-0.11}$
HD 37357	796 $^{+297}_{-175}$	0.97 $^{+0.13}_{-0.11}$	1.69 $^{+0.87}_{-0.93}$	3.92 $^{+0.18}_{-0.16}$	3 $^{+1}_{-0.4}$
HD 37490	320 $^{+45}_{-35}$	0.1 $^{+0.01}_{-0.01}$	0.1 $^{+0.11}_{-0.07}$	9.16 $^{+0.29}_{-0.23}$	8.6 $^{+3.9}_{-1.6}$

Table 1
(Continued)

Object	Distance (pc)	Age (Myr)	V18 Age (Myr)	Mass (M_{\odot})	V18 Mass (M_{\odot})
HD 37806	423 ⁺¹¹ ₋₁₀	1.65 ^{+0.02} _{-0.02}	1.56 ^{+0.64} _{-0.6}	3.28 ^{+0.02} _{-0.02}	3.11 ^{+0.55} _{-0.33}
HD 38120	402 ⁺¹⁴ ₋₁₃	2.62 ^{+0.1} _{-0.1}	3 ⁺¹⁴ ₋₁	2.96 ^{+0.07} _{-0.07}	2.37 ^{+0.43} _{-0.24}
HD 53367	131 ⁺¹⁶ ₋₁₃
HD 59319	660 ⁺²² ₋₂₁	1.12 ^{+0.02} _{-0.02}	0.96 ^{+0.24} _{-0.2}	3.93 ^{+0.02} _{-0.02}	3.81 ^{+0.31} _{-0.26}
HD 68695	392 ⁺⁶ ₋₆	7.3 ^{+0.05} _{-0.06}	7.6 ^{+1.1} _{-1.2}	2.08 ^{+0.01} _{-0.01}	1.833 ^{+0.092} _{-0.092} ^a
HD 72106	2552 ⁺²¹⁴¹ ₋₁₂₅₆	<0.1	2.1 ^{+2.6} _{-1.5}	9.06 ^{+0.81} _{-0.73}	2.7 ^{+1.5} _{-0.7}
HD 76534	895 ⁺³¹ ₋₂₉	0.27 ^{+0.01} _{-0.01}	0.171 ^{+0.023} _{-0.028} ^a	6.31 ^{+0.05} _{-0.05}	7.46 ^{+0.51} _{-0.37}
HD 85567	1002 ⁺³⁰ ₋₂₈	<0.1	0.217 ^{+0.045} _{-0.051} ^a	11.4 ^{+0.1} _{-0.1}	6.32 ^{+0.53} _{-0.39}
HD 87403	2038 ⁺²⁰³ ₋₁₇₀	0.19 ^{+0.01} _{-0.01}	0.28 ^{+0.11} _{-0.08}	6.72 ^{+0.08} _{-0.08}	5.51 ^{+0.65} _{-0.53}
HD 94509	1857 ⁺¹²⁷ ₋₁₁₂	...	0.28 ^{+0.17} _{-0.12}	...	5.7 ^{+1.1} _{-0.8}
HD 95881	1148 ⁺⁴⁶ ₋₄₂	0.16 ^{+0.01} _{-0.01}	0.28 ^{+0.05} _{-0.07}	7.06 ^{+0.04} _{-0.04}	5.5 ^{+0.5} _{-0.27}
HD 96042	4007 ⁺⁶⁴⁹ ₋₄₉₇	<0.1	0.019 ^{+0.008} _{-0.005}	20.09 ^{+0.49} _{-0.46}	20.7 ^{+3.9} _{-2.9}
HD 97048	184 ⁺¹ ₋₁	3.48 ^{+0.01} _{-0.02}	4.4 ^{+1.1} _{-0.3}	2.52 ^{+0.01} _{-0.01}	2.25 ^{+0.11} _{-0.13}
HD 98922	678 ⁺¹⁶ ₋₁₅	0.15 ^{+0.01} _{-0.01}	0.204 ^{+0.01} _{-0.038} ^a	7.42 ^{+0.02} _{-0.04}	6.17 ^{+0.37} _{-0.31}
Hen 3-1191	1959 ⁺³²⁷ ₋₂₄₇	0.38 ^{+0.03} _{-0.02}	0.23 ^{+0.37} _{-0.11}	4.96 ^{+0.1} _{-0.1}	8.1 ^{+2.1} _{-0.4}
IP Per	305 ⁺⁸ ₋₇	11.3 ^{+0.24} _{-0.25}	12 ⁺⁸ ₋₃	1.74 ^{+0.01} _{-0.01}	1.56 ^{+0.11} _{-0.12}
LkHA 167	1176 ⁺¹⁴¹ ₋₁₁₄	0.19 ^{+0.01} _{-0.01}	18.5 ^{+1.5} _{-1.4}	6.18 ^{+0.1} _{-0.11}	1.513 ^{+0.076} _{-0.076} ^a
LkHA 208	676 ⁺¹¹⁵ ₋₈₆	4.17 ^{+0.23} _{-0.22}	9 ⁺¹¹ ₋₅	2.28 ^{+0.04} _{-0.05}	1.56 ^{+0.47} _{-0.14}
LkHA 218	1104 ⁺⁴⁶ ₋₄₃	2.02 ^{+0.04} _{-0.04}	5 ⁺¹⁵ ₋₁	3.01 ^{+0.02} _{-0.02}	2.12 ^{+0.19} _{-0.12}
LkHA 220	1162 ⁺⁵⁶ ₋₅₁	1.57 ^{+0.05} _{-0.05}	2.04 ^{+0.34} _{-0.15}	3.54 ^{+0.06} _{-0.05}	3.02 ^{+0.15} _{-0.15}
LkHA 224	1253 ⁺²⁴⁹ ₋₁₈₀	0.29 ^{+0.07} _{-0.06}	1.2 ^{+1.1} _{-0.6}	5.52 ^{+0.28} _{-0.12}	2.85 ^{+0.72} _{-0.55}
LkHA 234	901 ⁺¹⁹ ₋₁₈	0.32 ^{+0.04} _{-0.04}	1.63 ^{+0.75} _{-0.6}	6.38 ^{+0.38} _{-0.3}	3.18 ^{+0.51} _{-0.39}
LkHA 25	868 ⁺¹¹² ₋₈₉	...	6 ⁺¹⁴ ₋₁	...	2.3 ^{+0.13} _{-0.11}
LkHA 257	777 ⁺¹⁰ ₋₁₀	7.39 ^{+0.03} _{-0.03}	3.6 ^{+1.1} _{-1.1}	1.82 ^{+0.01} _{-0.01}	3.08 ^{+0.15} _{-0.15}
LkHA 259	743 ⁺¹⁹ ₋₁₈	1.24 ^{+0.02} _{-0.02}	6.4 ^{+1.6} _{-0.9}	3.43 ^{+0.02} _{-0.02}	1.7 ^{+0.1} _{-0.13}
LkHa 339	839 ⁺¹⁹ ₋₁₈	2.37 ^{+0.03} _{-0.04}	2.54 ^{+0.23} _{-0.16}	3 ^{+0.03} _{-0.03}	2.59 ^{+0.13} _{-0.13}
MWC 1080	1336 ⁺¹⁹⁹ ₋₁₅₄	...	0.04 ^{+0.45} _{-0.02}	...	16.1 ^{+6.3} _{-4.2}
MWC297	372 ⁺¹² ₋₁₂	...	0.027 ^{+0.006} _{-0.006} ^a	...	16.9 ^{+1.2} _{-1.2}
PDS 124	843 ⁺³⁶ ₋₃₃	4.98 ^{+0.06} _{-0.07}	6 ⁺¹⁴ ₋₁	2.16 ^{+0.01} _{-0.01}	2.07 ^{+0.1} _{-0.12}
PDS 130	1278 ⁺³⁴ ₋₃₃	2.02 ^{+0.02} _{-0.04}	3.48 ^{+0.27} _{-0.26}	3.12 ^{+0.01} _{-0.01}	2.33 ^{+0.12} _{-0.12}
PDS 133	1437 ⁺⁵¹ ₋₄₈	4.88 ^{+0.4} _{-0.43}	3 ⁺¹⁴ ₋₁	2.01 ^{+0.06} _{-0.04}	2.93 ^{+0.45} _{-0.44}
PDS 134	2802 ⁺²⁹¹ ₋₂₄₂	0.37 ^{+0.02} _{-0.02}	0.73 ^{+0.22} _{-0.21}	5.62 ^{+0.04} _{-0.04}	4.28 ^{+0.52} _{-0.38}
PDS 144S	149 ⁺³ ₋₃
PDS 174	393 ⁺⁶ ₋₆	3.11 ^{+0.04} _{-0.05}	2 ⁺¹⁸ ₋₁	2.69 ^{+0.02} _{-0.02}	2.71 ^{+0.36} _{-0.23}
PDS 24	1099 ⁺²³ ₋₂₃	6.41 ^{+0.06} _{-0.14}	10 ⁺¹⁰ ₋₄	2.22 ^{+0.02} _{-0.02}	1.95 ^{+0.1} _{-0.1}
PDS 241	5259 ⁺¹⁵³⁵ ₋₁₀₅₇	<0.1	0.078 ^{+0.036} _{-0.028} ^a	23.01 ^{+0.95} _{-0.94}	11.1 ^{+2.3} _{-1.3}
PDS 27	3262 ⁺⁵⁷⁰ ₋₄₂₈	<0.1	0.042 ^{+0.072} _{-0.027} ^a	>25	12.2 ^{+5.5} _{-3.4}
PDS 281	914 ⁺²⁷ ₋₂₅	<0.1	...	10.06 ^{+0.06} _{-0.04}	...
PDS 286	1838 ⁺¹²⁶ ₋₁₁₁	...	0.011 ^{+0.006} _{-0.001} ^a	...	31.2 ^{+4.5} _{-5.5}
PDS 33	931 ⁺²⁴ ₋₂₃	7.16 ^{+0.16} _{-0.17}	10.7 ^{+9.3} _{-3.9}	2.04 ^{+0.01} _{-0.01}	1.85 ^{+0.093} _{-0.093} ^a
PDS 344	2360 ⁺⁹⁶ ₋₈₉	2.38 ^{+0.04} _{-0.03}	1.8 ^{+8.4} _{-0.2}	2.89 ^{+0.02} _{-0.02}	3.48 ^{+0.17} _{-0.23}
PDS 361S	3378 ⁺³⁸⁹ ₋₃₁₈	0.19 ^{+0.01} _{-0.01}	0.6 ^{+3.8} _{-0.3}	7.81 ^{+0.11} _{-0.11}	5 ⁺¹ _{-0.7}
PDS 37	2260 ⁺³⁴² ₋₂₆₄	...	0.06 ^{+0.1} _{-0.03}	...	10.9 ^{+4.5} ₋₃
PDS 415N	144 ⁺³ ₋₃	...	13.1 ^{+5.4} _{-4.5}	...	1.21 ^{+0.16} _{-0.09}
PDS 431	1787 ⁺⁹⁰ ₋₈₂	1.59 ^{+0.03} _{-0.03}	2.77 ^{+0.45} _{-0.73}	3.46 ^{+0.03} _{-0.02}	2.52 ^{+0.27} _{-0.15}
PDS 69	689 ⁺¹⁹ ₋₁₈	0.95 ^{+0.02} _{-0.01}	0.8 ^{+5.6} _{-0.3}	3.96 ^{+0.02} _{-0.02}	4.18 ^{+0.73} _{-0.51}
R CrA	96 ⁺⁷ ₋₆
RR Tau	763 ⁺²⁸ ₋₂₆	1.7 ^{+0.2} _{-0.64}	1.98 ^{+0.4} _{-0.69}	3.28 ^{+1.23} _{-0.14}	2.82 ^{+0.46} _{-0.19}
SV Cep	341 ⁺² ₋₂	4.6 ^{+0.24} _{-0.04}	6 ⁺¹³ ₋₁	2.48 ^{+0.11} _{-0.02}	1.55 ^{+0.077} _{-0.077} ^a
T Ori	403 ⁺⁷ ₋₇	4.64 ^{+0.36} _{-0.34}	4.15 ^{+0.56} _{-0.67}	2.18 ^{+0.06} _{-0.06}	2.11 ^{+0.14} _{-0.11}
TY CrA	136 ⁺³ ₋₃	5.39 ^{+0.04} _{-0.05}	6 ⁺¹⁴ ₋₂	2.09 ^{+0.02} _{-0.01}	2.06 ^{+0.22} _{-0.19}
TYC 8581-2002-1	549 ⁺⁷ ₋₇	3.36 ^{+0.02} _{-0.04}	8 ⁺¹² ₋₁	2.99 ^{+0.05} _{-0.05}	1.88 ^{+0.094} _{-0.094} ^a
TYC 8593-2802-1	1570 ⁺⁸¹ ₋₇₄	3.23 ^{+0.06} _{-0.06}	1.75 ^{+0.63} _{-0.35}	2.43 ^{+0.02} _{-0.02}	2.99 ^{+0.27} _{-0.31}
UX Ori	322 ⁺⁵ ₋₅	8.22 ^{+0.27} _{-0.26}	11.4 ^{+8.6} _{-2.7}	1.74 ^{+0.05} _{-0.02}	1.612 ^{+0.091} _{-0.081} ^a
UY Ori	353 ⁺¹¹ ₋₁₀
VI012 Ori	383 ⁺⁸ ₋₇	...	8.5 ^{+1.1} _{-0.9}	...	1.3 ^{+0.065} _{-0.065} ^a
VI028 Cen	997 ⁺³⁷⁹ ₋₂₁₈	2.28 ^{+0.26} _{-0.25}	2.4 ^{+8.5} _{-1.1}	2.93 ^{+0.13} _{-0.11}	3 ^{+0.6} _{-0.15}
V1308 Ori	5523 ⁺¹⁷³⁰ ₋₁₁₆₈	...	0.018 ^{+0.019} _{-0.008} ^a	...	23 ⁺¹¹ ₋₇

Table 1
(Continued)

Object	Distance (pc)	Age (Myr)	V18 Age (Myr)	Mass (M_{\odot})	V18 Mass (M_{\odot})
V1366 Ori	309^{+5}_{-5}	...	$6.5^{+2.4}_{-0.6}$...	$1.45^{+0.072}_{-0.072}$ ^a
V1787 Ori	387^{+8}_{-8}	$0.57^{+0.02}_{-0.02}$	$7.4^{+0.6}_{-1.1}$	$2.04^{+0.03}_{-0.02}$	$1.659^{+0.094}_{-0.083}$ ^a
V346 Ori	363^{+6}_{-6}	$8.23^{+0.17}_{-0.17}$	$9.33^{+0.47}_{-0.47}$	$1.89^{+0.01}_{-0.01}$	$1.572^{+0.079}_{-0.079}$ ^a
V350 Ori	389^{+19}_{-18}	$9.96^{+1.29}_{-1.5}$	$12.2^{+7.8}_{-4.7}$	$1.8^{+0.08}_{-0.06}$	$1.706^{+0.094}_{-0.085}$ ^a
V380 Ori	486^{+42}_{-36}	$0.51^{+0.02}_{-0.02}$	$2^{+1}_{-0.8}$	$5.04^{+0.08}_{-0.05}$	$2.82^{+0.59}_{-0.38}$
V599 Ori	406^{+7}_{-7}	$0.36^{+0.05}_{-0.05}$	$4.29^{+0.42}_{-0.54}$	$2.17^{+0.15}_{-0.15}$	$2.03^{+0.1}_{-0.1}$
V699 Mon	703^{+23}_{-22}	$0.53^{+0.02}_{-0.01}$	$0.96^{+0.44}_{-0.3}$	$4.99^{+0.03}_{-0.04}$	$4^{+0.49}_{-0.48}$
V791 Mon	872^{+30}_{-28}	$0.92^{+0.01}_{-0.02}$	$1^{+3.1}_{-0.3}$	$4.28^{+0.04}_{-0.04}$	$3.94^{+0.51}_{-0.45}$
V856 Sco	160^{+2}_{-2}	$3.88^{+0.66}_{-1.22}$...	$2.22^{+0.24}_{-0.07}$...
V892 Tau	117^{+2}_{-2}
VV Ser	415^{+8}_{-8}	$0.9^{+0.12}_{-0.37}$	$2.8^{+8.1}_{-0.2}$	$4.37^{+1.35}_{-0.36}$	$2.89^{+0.14}_{-0.14}$
VX Cas	529^{+11}_{-10}	...	9^{+11}_{-4}	...	$1.88^{+0.18}_{-0.09}$
WW Vul	497^{+9}_{-9}	$3.3^{+0.06}_{-0.06}$	$5.08^{+0.84}_{-0.71}$	$2.58^{+0.04}_{-0.03}$	$1.95^{+0.11}_{-0.1}$
XY Per	456^{+19}_{-18}	$1.56^{+0.04}_{-0.05}$	$1.95^{+0.43}_{-0.44}$	$3.31^{+0.03}_{-0.04}$	$2.82^{+0.29}_{-0.2}$
Z CMa	253^{+118}_{-61}	...	$0.8^{+0.83}_{-0.59}$...	$3.8^{+2}_{-0.8}$

Notes. The columns in the table include object name, distance, age (our work), age (Vioque et al. 2018—V18), mass (our work), and mass (V18). Our estimates of age and mass are derived using the *Gaia* CMD.

^a The errors in our age and mass estimates are rounded off to two digits whereas those from Vioque et al. (2018) are reproduced as in their paper.

(This table is available in machine-readable form.)

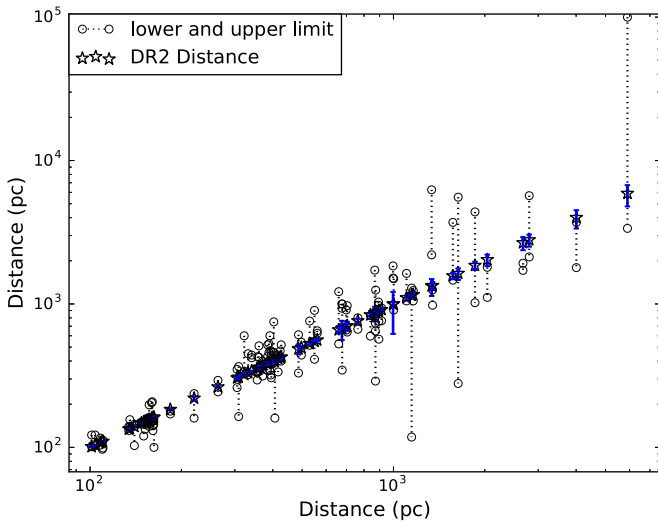


Figure 1. Comparison between the distances of H AeBe stars from the *Gaia* DR2 with the values from previous studies. The distance of the H AeBe stars in parsec is shown in both the axes. Distance estimated from the *Gaia* DR2 parallax, using the method outlined in Section 3.1, is shown as star symbols, with the error indicated by the blue line. The lower and upper bound values of distance for each star are compiled from the literature and are shown as two open circles connected by a dotted line.

Using these relations we estimated A_G , $A_{G_{BP}}$, and $A_{G_{RP}}$ from the known values of A_V . This is further used to correct the *Gaia* magnitudes, which will be used for this work.

3.3. Age and Mass of H AeBe Stars

In addition to precise astrometric measurements, the *Gaia* DR2 lists three broadband photometric magnitudes, G , G_{BP} , and G_{RP} , extinction in the G band (A_G), and reddening ($E(G_{BP} - G_{RP})$) values. This provides the possibility to construct a CMD exclusively from *Gaia* magnitudes (Gaia Collaboration et al. 2018a). We identified that the G -band filter in *Gaia* is very wide (720 nm) and hence can introduce

uncertainty in G -magnitude measurements. Hence for the present work, we use G_{BP} and G_{RP} magnitudes for constructing the CMD. The observed *Gaia* G_{BP} and G_{RP} are corrected for extinction using the method discussed in Section 3.2. Further, making use of the distance estimates (see Table 1), we estimated the absolute G_{RP} magnitude ($M_{G_{RP}}$), which will be used for the CMD analysis. Usually, the construction of the CMD with non-homogeneous data sets belonging to different epochs can introduce systematic errors in the estimation of stellar parameters. The use of *Gaia* astrometry and photometry for the CMD analysis alleviate this issue. Also, we derived the age and mass of H AeBe stars from the observed CMD rather than from a theoretical Hertzsprung–Russell (HR) diagram. The luminosity calculation for stars in the HR diagram involves the conversion of the V magnitude to luminosity using bolometric corrections. Such a conversion will provide substantial errors in mass and age estimates. In addition, the effective temperature of the star (T_{eff}) is identified using a calibration table that introduces degeneracy in T_{eff} for relatively nearer spectral types.

The age and mass of the H AeBe stars are estimated by plotting Modules for Experiments in Stellar Astrophysics (MESA) isochrones and evolutionary tracks (MIST⁴; Choi et al. 2016; Dotter 2016) in the *Gaia* CMD. The MIST is an initiative supported by the National Science Foundation (NSF), NASA, and Packard Foundation, which build stellar evolutionary models with different ages, masses, and metallicities. The updated models in the MIST archive included isochrones and evolutionary tracks for the *Gaia* DR2 data. We know that H AeBe stars have a range of rotation rates but we adopted the isochrones corresponding to $(V/V_{\text{crit}}) = 0.4$, since that is the only model available in the MIST database for a rotating system. Also, we adopted the metallicity of $\left[\frac{\text{Fe}}{\text{H}}\right] = 0$ (corresponding to solar metallicity; $Z_{\odot} = 0.0152$) for estimating the age and mass of H AeBe stars.

⁴ <http://waps.cfa.harvard.edu/MIST/>

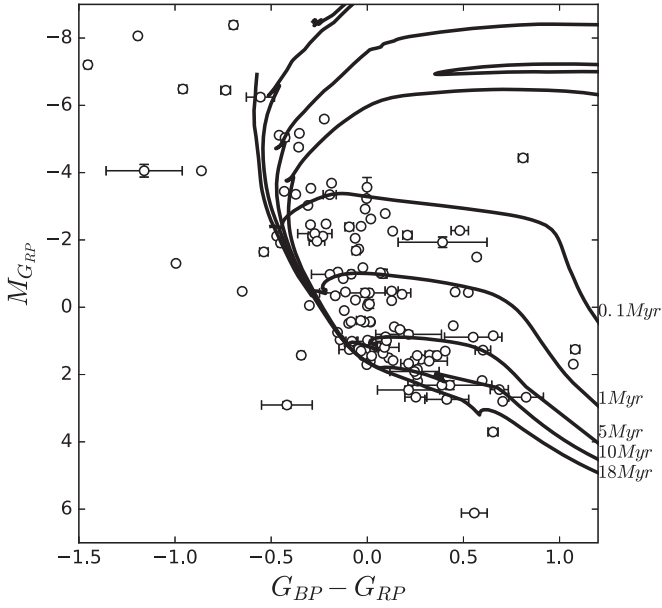


Figure 2. MIST isochrones overplotted on the *Gaia* CMD containing 131 H AeBe stars. Isochrones of ages from 0.1 to 18 Myr are plotted in the CMD with metallicity, $Z_{\odot} = 0.0152$ and $(V/V_{\text{crit}}) = 0.4$.

The *Gaia* CMD for our sample of 131 H AeBe stars is shown in Figures 2 and 3. From Figure 2, we estimated the ages of 110 H AeBe stars by overplotting the MIST isochrones. They are found to be in the range of 0.1–15 Myr. From Figure 3, it can be seen that the mass range of our sample of H AeBe stars is 1.4–25 M_{\odot} . The masses are identified from the coincidence of the data points with the grid of MIST evolutionary tracks. The estimated ages and masses of the H AeBe stars from this work are compared with that in Vioque et al. (2018) and are listed in Table 1. We found that 21 stars from our sample are placed below the main sequence and hence the parameters could not be estimated. Since these stars are cataloged as H AeBe stars, they may be properly positioned in the PMS location in previous studies. H AeBe stars are known to show photometric variability (van den Ancker et al. 1998). The stars which are found below the main sequence in Figures 2 and 3 may show photometric variability. Also, some stars are positioned in the evolved region of the evolutionary track. Further studies are needed to evaluate the nature of these candidates.

3.4. Mass Accretion Rates of H AeBe Stars

The mass accretion process during the PMS phase represents one of the important mechanisms associated with star formation. In T Tauri stars, mass accretion is through a process known as magnetospheric accretion (MA) in which the magnetosphere of the host star truncates the circumstellar disk at a few stellar radii and the material from the disk fall onto the star at freefall velocities along the magnetic field lines, which in turn create shocks at the surface of the star. The hot (10^4 K) emission from the post-shock gas appear as excess in the UV continuum of T Tauri stars (e.g., Calvet & Gullbring 1998; Gullbring et al. 1998; Hartmann et al. 1998; Bouvier et al. 2007). The MA accretion model may not be a viable mode of accretion in H AeBe stars since there are no convincing signatures of a magnetic field in these systems (Alecian et al. 2013). Although many studies

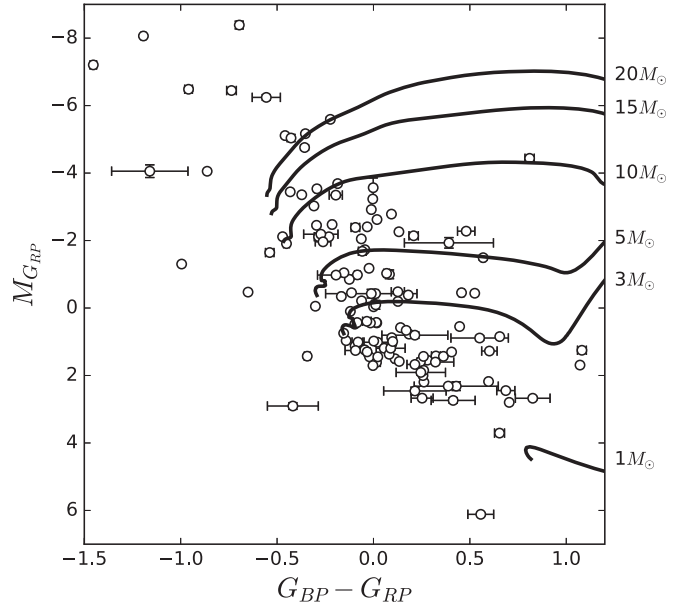


Figure 3. *Gaia* CMD containing 131 H AeBe stars overplotted with the MIST evolutionary tracks. Evolutionary tracks with masses ranging from 1 to 20 M_{\odot} are plotted in the CMD. We used the MIST tracks with metallicity, $Z_{\odot} = 0.0152$ and $(V/V_{\text{crit}}) = 0.4$.

suggest disk accretion as the possible mechanism in Herbig Be stars, a consensus is yet to be obtained whether MA accretion can account for mass accretion in low-mass H AeBe stars (Muzerolle et al. 2004). For the present work, we employed MA formalism while calculating the \dot{M}_{acc} in H AeBe stars.

The $H\alpha$ line flux values of 102 H AeBe stars are taken from Mathew et al. (2018), Fairlamb et al. (2017), and Mendigutía et al. (2011b). In addition, we took the $H\alpha$ equivalent width (EW) for four stars from Boehm & Catala (1995), Baines et al. (2006), Borges Fernandes et al. (2007), and Vieira et al. (2011). The EW is converted to line flux from the R -band magnitude using the method mentioned in Mathew et al. (2018). Hence, for the present analysis, we will be using the $H\alpha$ line flux ($F_{H\alpha}$) values of 106 H AeBe stars. The $H\alpha$ line flux is converted to luminosity ($L_{H\alpha}$) using the equation

$$L_{H\alpha} = 4\pi d^2 F_{H\alpha}, \quad (4)$$

where d is the distance in parsec. The accretion luminosity (L_{acc}) is calculated using the empirical relation given in Fairlamb et al. (2017), which is reproduced as

$$\log \frac{L_{\text{acc}}}{L_{\odot}} = 2.09(\pm 0.06) + 1.00(\pm 0.05) \times \log \frac{L_{H\alpha}}{L_{\odot}}. \quad (5)$$

The (\dot{M}_{acc}) can be derived from the L_{acc} using the relation

$$L_{\text{acc}} = \frac{GM_* \dot{M}_{\text{acc}}}{R_*} \left(1 - \frac{R_i}{R_*} \right), \quad (6)$$

where M_* is the mass of H AeBe stars, estimated in Section 3.3 and given in Table 1 and R_i is the disk truncation radius. For T Tauri stars, R_i is assumed to be $5 R_*$ (Gullbring et al. 1998; Costigan et al. 2014). H AeBe stars are fast rotators and therefore have a smaller co-rotation radius. The disk truncation radius, R_i , should be smaller than the co-rotation radius (Shu et al. 1994). Thus in this work, we adopt a disk truncation

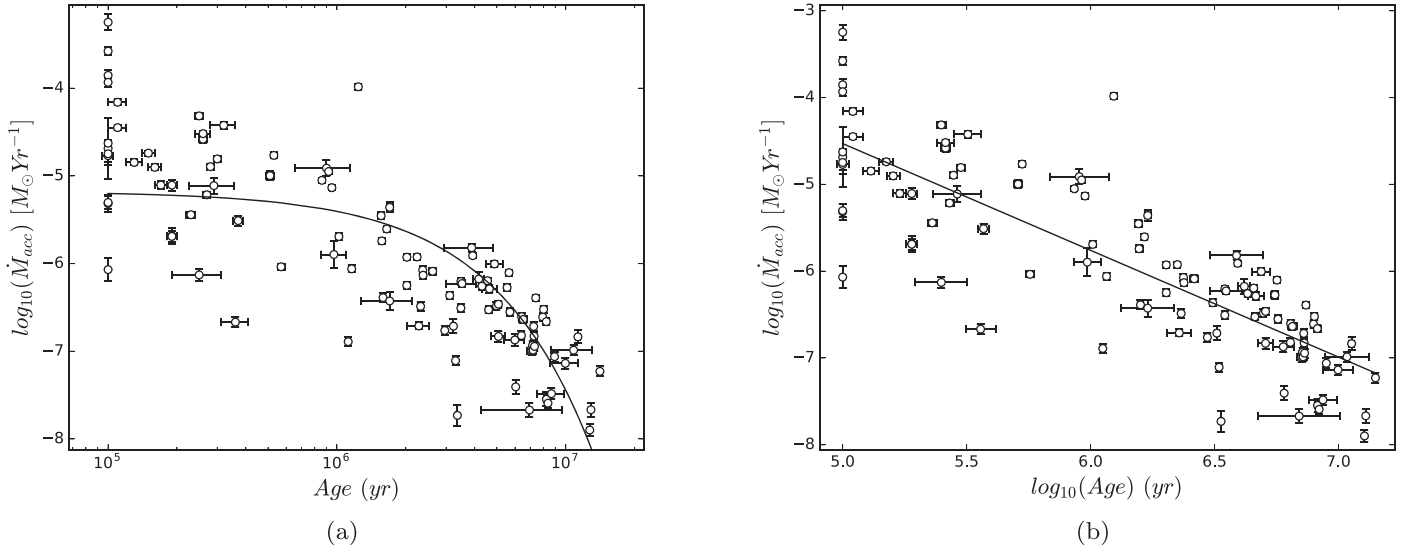


Figure 4. Relationship between $\log(\dot{M}_{\text{acc}})$ and age (t) in years for a sample of 106 H AeBe stars. Panel (a) shows an exponential decrease in $\log(\dot{M}_{\text{acc}})$ with age for H AeBe stars, as expressed in Equation (8). The best fit gives $\tau = 1.9 \pm 0.1$ Myr illustrated with a solid line. Panel (b) depicts a log–log plot of \dot{M}_{acc} with age. The power-law relation given by Equation (9) gives a value of $\eta = 1.2 \pm 0.1$, which is represented by a solid line.

radius of $R_i = 2.5 R_*$ (Muzerolle et al. 2004; Mendigutía et al. 2011a; Fairlamb et al. 2015). The stellar radius R_* for the 106 H AeBe stars are calculated using the equation

$$R_* = \left(\frac{L_*}{4\pi\sigma T_{\text{eff}}^4} \right)^{1/2}, \quad (7)$$

where L_* is the bolometric luminosity of the star, which is calculated from the V magnitude, bolometric correction, and *Gaia* distance. Using the calibration table listed in Pecaut & Mamajek (2013), we identified the T_{eff} and bolometric correction corresponding to the spectral type of the H AeBe star. The V magnitudes of 101 H AeBe stars are compiled from American Association of Variable Star Observers (AAVSO) Photometric All-sky Survey (Henden et al. 2016) and Tycho-2 (Høg et al. 2000) catalogs. The remaining five stars which had no V magnitude listed in both the catalogs are taken from Herbst & Shevchenko (1999), Getman et al. (2008), Fresneau & Osborn (2009), and Girard et al. (2011).

3.5. Correlation Analysis of Mass Accretion Rates with Stellar Parameters

The relationship between the \dot{M}_{acc} and the stellar parameters such as age and mass are analyzed in some of the studies (e.g., Mendigutía et al. 2011a, 2015; Fairlamb et al. 2017). However, in the context of precise mass and age estimates using *Gaia* DR2, we re-assessed the relations between \dot{M}_{acc} and the stellar parameters using the largest sample of 106 H AeBe stars to date. Figure 4(a) illustrates the correlation between the $\log(\dot{M}_{\text{acc}})$ and age of H AeBe stars. It can be seen that $\log(\dot{M}_{\text{acc}})$ decays exponentially with the age of H AeBe stars. This trend is discussed in the studies of Manoj et al. (2006) and Mendigutía et al. (2012). From the rate of decline of the accretion rate, it is possible to estimate the disk dissipation timescale, τ , using the relation

$$\dot{M}_{\text{acc}}(t) = \dot{M}_{\text{acc}}(0)e^{-t/\tau}, \quad (8)$$

where t is the age of the H AeBe stars. By fitting the relation to the set of data points, we obtained the disk dissipation timescale, $\tau = 1.9 \pm 0.1$ Myr. This value is near to that given in Mendigutía et al. (2012), which is $\tau = 1.3^{+1.0}_{-0.5}$ Myr. It may be noted that τ for T Tauri stars is 2–4 Myr (Fedele et al. 2010; Takagi et al. 2014). We find a lower τ value for the H AeBe stars indicating that the disk dissipation timescale is shorter for intermediate-mass young stars compared to their lower mass counterparts.

Further, another parameter used in the literature for calculating the rate of decline of the accretion rate with age in YSOs is the power-law index, η (Hartmann et al. 1998; Mendigutía et al. 2012; Fairlamb et al. 2015). The relation which connects \dot{M}_{acc} with the age of the star can also be considered as a power-law distribution of the form

$$\dot{M}_{\text{acc}} = \text{constant} \times t^{-\eta}. \quad (9)$$

From the best fit to the distribution of the data points in Figure 4(b), we obtained $\eta = 1.2 \pm 0.1$. This value is on the lower end when compared to the estimates of Mendigutía et al. (2012) and Fairlamb et al. (2015), which are $1.8^{+1.3}_{-0.7}$ and 1.92 ± 0.09 , respectively. This could be because of the increased number of high-mass HBe stars in our sample.

In Figure 5 we plotted the correlation between \dot{M}_{acc} and stellar mass. Our sample of H AeBe stars covers a broader range in spectral type/mass and \dot{M}_{acc} ($\sim 10^{-3}$ – $10^{-7} M_{\odot} \text{yr}^{-1}$), when compared to the sample of stars given in Mendigutía et al. (2011a). This is because our sample contains high-mass candidates with a mass $> 6 M_{\odot}$, whereas those listed in Mendigutía et al. (2011a) are with a mass $< 6 M_{\odot}$. The best fit for our sample of H AeBe stars in Figure 5 provides the relation $\dot{M}_{\text{acc}} \propto M_*^{2.8 \pm 0.2}$. Mendigutía et al. (2011a) did a similar study and obtained a steep power-law relation, $\dot{M}_{\text{acc}} \propto M_*^5$. The reason for a steeper power-law relation might be due to the unavailability of massive H AeBe stars in their sample. The Pearson correlation coefficient for our fit is 0.81 for a sample size of 106 stars. Incidentally, Fairlamb et al. (2015) obtained the relation between stellar mass and accretion rate as $\dot{M}_{\text{acc}} \propto M_*^{3.72 \pm 0.27}$, which comes close to our estimate. It

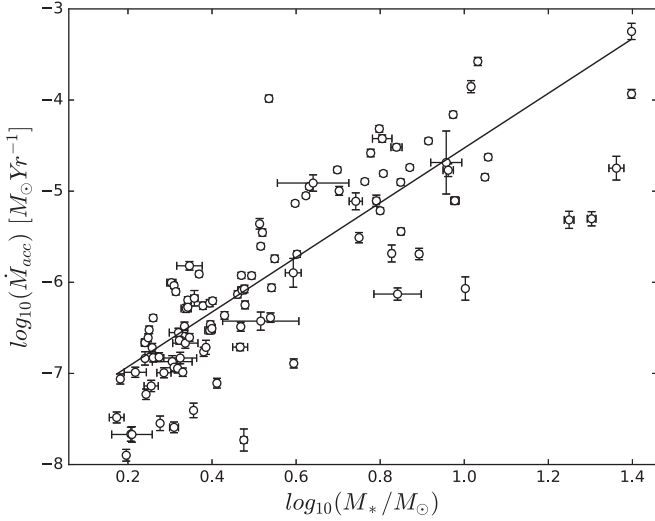


Figure 5. Log–log plot of \dot{M}_{acc} and the stellar mass for a sample of 106 H AeBe stars. The solid line shows the best fit for the power-law relation between \dot{M}_{acc} and the stellar mass in H AeBe stars. The power-law index estimated from the best fit is 2.8 ± 0.2 .

may be noted that the mass dependence of accretion rate in T Tauri stars is lower than the value calculated for H AeBe stars, i.e., $\dot{M}_{\text{acc}} \propto M_*^2$ (Muzerolle et al. 2005; Natta et al. 2006).

The best fit and the confidence limits for Figures 4(a), (b), and 5 are determined using the Monte Carlo method to account for the associated uncertainties in age, mass, and \dot{M}_{acc} . For this purpose, 100,000 samples for age, mass, and \dot{M}_{acc} were created. The values for these samples were randomly drawn from a Gaussian distribution having a mean equal to the actual measured value in each case and a standard deviation equal to the associated uncertainty. The best fit is then estimated for each of the resulting data sets. The fit parameters obtained for all 100,000 data sets results in a normal distribution, the mean of which, along with its 3σ confidence limits, is taken as the final best fit.

3.6. Quantifying IR Excess Using Spectral Index

Infrared excess in the spectral energy distribution (SED) is one of the important criterion used in identifying YSOs. It provides a better understanding of the composition of gas and dust in the disk of a PMS star. Lada & Wilking (1984) differentiated YSOs into different classes from the shape of their SEDs in the IR region. Lada (1987) quantified the classification scheme using the slope in the IR region of the SED, which are known as Lada indices. The YSOs can be classified as Class 0, Class I, Class II, and Class III, based on the steepness of the indices at various wavelength intervals (Lada 1987; Andre et al. 1993). The estimation and analysis of Lada indices are very important in studying the evolution of H AeBe stars as it gives an idea about the evolution of the CSM. The equation defining the spectral index (Lada 1987; Wilking 1989; Greene et al. 1994) is expressed as

$$n_{\lambda_1 - \lambda_2} = \frac{\log\left(\frac{\lambda_2 F_{\lambda_2}}{\lambda_1 F_{\lambda_1}}\right)}{\log\left(\frac{\lambda_2}{\lambda_1}\right)}. \quad (10)$$

For our analysis we consider the spectral index, $n_{2-4.6}$, which is the ratio of the flux values at the 2MASS (Skrutskie et al. 2006)

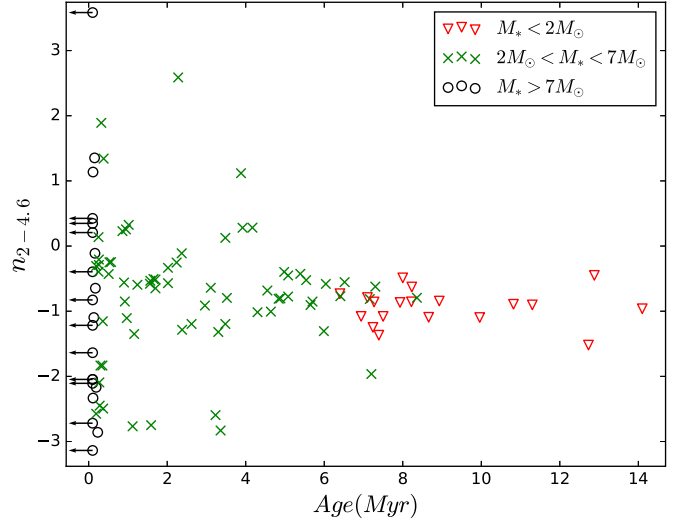


Figure 6. Graph between the age and spectral index of H AeBe stars. Stars having a mass less than $2 M_\odot$ are represented by red triangles. Stars having a mass between 2 and $7 M_\odot$ are represented by green crosses, while stars having a mass more than $7 M_\odot$ are shown as open circles. Arrows are assigned to the stars having an age upper limit of 0.1 Myr.

K_s -band (i.e., $\lambda_1 = 2.159 \mu\text{m}$) and *WISE* (Cutri et al. 2013) W2-band (i.e., $\lambda_2 = 4.6 \mu\text{m}$). The age estimates are available only for 110 stars. However, the spectral index is not calculated for the H AeBe stars CPD-61 3587B and LkHA 224 due to the unavailability of *WISE* magnitudes. Hence, a sample of 108 stars is used for this analysis.

A plot between spectral index ($n_{2-4.6}$) and age of H AeBe stars is shown in Figure 6. No clear trend is evident in the variation of $n_{2-4.6}$ with respect to age in Figure 6. However, when we categorize the H AeBe stars in various mass bins, a tentative trend seems to emerge. For H AeBe stars with mass less than $2 M_\odot$, the $n_{2-4.6}$ value is around -1 . For stars in the mass range of $2-7 M_\odot$, there is a scatter in the distribution of $n_{2-4.6}$ values, with majority of the data points around $n_{2-4.6} = -1$. The majority of massive stars (mass $> 7 M_\odot$) are showing IR index from 0.5 to -3 , where the negative index is more prominent in these high-mass candidates. This agrees with the study of Alonso-Albi et al. (2009) where they suggested that in high-mass HBe stars disk dispersal is faster and disk masses are 5–10 times lesser than low-mass counterparts. They explained this observation by suggesting that the photoevaporation mechanism due to the UV radiation disperses the gas content in the disk, after which only a thin dusty disk containing large grains remains. The caveat in our study is the upper bound in age quoted for massive HBe stars.

3.7. Comparison with Vioque et al. (2018)

Calculation of stellar parameters from the theoretical HR diagram involves the use of derived variables such as bolometric luminosity (L_{bol}) and effective temperature (T_{eff}). The estimation of these quantities from magnitude and color/spectral type involves approximations and comparison with standard calibration tables, which add more errors into the calculation of age and mass. Our analysis is based on the *Gaia* CMD rather than a theoretical HR diagram. Using a uniform photometric system combined with precise distances can give an accurate estimation of the age and mass of PMS stars. Thus, combining the refined stellar distances and the most consistent

photometric measurements from the *Gaia* DR2, along with the help of synthetic photometry isochrones and evolutionary tracks from the MIST, accurate stellar ages and masses are estimated in this work. In comparison, Vioque et al. (2018) adopted the theoretical HR diagram for the analysis of age and mass. The differences between our analysis with that of Vioque et al. (2018) are listed below.

1. We used the photometry and distances from *Gaia* for the estimation of the age and mass of HAeBe stars. Vioque et al. (2018) used only the *Gaia* distances for the same.
2. Vioque et al. (2018) used the distance estimation method outlined in Bailer-Jones et al. (2018) and the calculated that the distances have high error bars than the values listed in the catalog released by Bailer-Jones et al. (2018). We used the distances listed in the catalog of Bailer-Jones et al. (2018). For example, the distance of star DG Cir from Bailer-Jones et al. (2018) is 821^{+30}_{-28} pc. For the same star Vioque et al. (2018) estimated a distance of 833^{+52}_{-43} pc.
3. We used $R_V = 5$ for the A_V calculation of HAeBe stars whereas Vioque et al. (2018) used $R_V = 3.1$. This is because Hernández et al. (2004) showed that total to selective extinction, $R_V = 5$ better reproduces the stellar parameters of HAeBe stars. Also, it is understood that the photometric variability and high value of reddening in HAeBe stars are not due to the interstellar medium, but due to dust particles with large grain size in the CSM (see Gorti & Bhatt 1993; Manoj et al. 2006).
4. For a statistical comparison of stellar parameters with Vioque et al. (2018), we also estimated ages and masses of HAeBe stars with $R_V = 3.1$. The median of the fractional difference between our ages with $R_V = 3.1$ and Vioque et al. (2018) ages is calculated to be within 19%. The fractional difference is defined as

$$\left| \frac{\text{Vioque estimate} - \text{Our estimate}}{\text{Our estimate}} \right| \times 100.$$

For masses, the fractional difference is found to be within 8%. The difference in age and mass could be due to our use of the *Gaia* CMD and the MIST models whereas Vioque et al. (2018) used the HR diagram and the Padova & Trieste Stellar Evolution Code (PARSEC) models (Bressan et al. 2012). This comparison is extended to our actual estimates of age and mass for $R_V = 5$. The median of the fractional difference of age and mass between our work ($R_V = 5$) and Vioque et al. (2018) is within 31% and 17%, respectively.

5. Vioque et al. (2018) used the $H\alpha$ EW for correlation studies with age and mass of HAeBe stars. However, for our analysis, we used the $H\alpha$ line flux, from which the \dot{M}_{acc} is calculated, which is used for the correlation analysis with the age and mass of HAeBe stars. It may be noted that Mendigutía et al. (2012) have reported that the $H\alpha$ EW may not give a clear idea about the gas content of the disk. They suggested estimating \dot{M}_{acc} from the $H\alpha$ line flux to study the gas content of the disk, which we employed in this work.
6. Vioque et al. (2018) used the continuum flux distribution from 1.24 to $22 \mu\text{m}$ for the analysis of the IR excess in HAeBe stars. This includes the flux measurement from the *WISE* W4 photometric band, which is not very reliable as the images of many HAeBe stars are not registered in

W4 band. Hence, we restricted the analysis to the *WISE* W2 band, which provides better photometry with good S/N and is free of artifacts.

7. Vioque et al. (2018) found that there is a break in IR excess with mass. We also arrived at a similar conclusion. However, they suggested considerably low IR excess for massive HAeBe stars whereas we see a considerable range in IR excess values in this work (see Figure 6).

4. Summary





The present study made use of the unprecedented capability of the *Gaia* mission to derive the stellar parameters such as the age and mass of HAeBe stars. Using the stellar parameters and the compiled $H\alpha$ flux, the \dot{M}_{acc} for the sample is estimated. Also, we investigated the capability of the IR spectral index as a better method in quantifying the IR excess. The main results of this study are summarized below.

1. Better accuracy of the *Gaia* DR2 astrometry is confirmed from the comparison of the *Gaia* DR2 distances with the previously estimated values from the literature. We adopted the distance values compiled in Bailer-Jones et al. (2018), which are the best distance estimates to date with minimal errors, for the sample of HAeBe stars used for this study.
2. The age and mass of 110 HAeBe stars are estimated using the *Gaia* CMD, with the aid of MIST isochrones and evolutionary tracks. To our knowledge, no studies were done until now which calculated the age and mass of a confirmed sample of HAeBe stars using both the photometry and distance from the *Gaia* mission. Since we employed *Gaia* CMD for estimating the age and mass of HAeBe stars, we avoided considerable errors when these quantities are estimated from theoretical HR diagram.
3. Mass accretion rates are calculated from the $H\alpha$ line flux measurements of 106 HAeBe stars, which is the largest sample to date. Since we had used distances and the stellar masses derived from *Gaia* DR2 data in the calculation of \dot{M}_{acc} , our estimates can be more accurate than previous studies.
4. The disk dissipation timescale derived for our sample of HAeBe stars is 1.9 ± 0.1 Myr, which is consistent with the previous estimate (Mendigutía et al. 2012).
5. We found that mass accretion rate is related to the mass of HAeBe stars in the form of the relation $\dot{M}_{\text{acc}} \propto M_*^{2.8 \pm 0.2}$.
6. We calculated the spectral index ($n_{2-4.6}$) in quantifying the IR excess in HAeBe stars. A correlation between the spectral index and age suggested a distinction between the disk of HAe and HBe stars. Massive HBe stars with ages < 0.1 Myr show diverse values of the IR spectral index, ranging from 0.5 to -3 , with the negative index being more prominent. The possibility of photoevaporation resulting in the dissipation of gas content in the disk, and thereby forming a thin disk and the formation difference between HBe and HAe stars, needs to be explored from further studies.

We would like to thank the anonymous referee for providing helpful comments and suggestions that improved the paper. This work has made use of data from the European Space Agency (ESA) mission *Gaia* (<https://www.cosmos.esa.int/gaia>),

processed by the Gaia Data Processing and Analysis Consortium (DPAC; <https://www.cosmos.esa.int/web/gaia/dpac/consortium>). Funding for the DPAC has been provided by national institutions, in particular, the institutions participating in the Gaia Multilateral Agreement. Some of the data presented in this paper were obtained from the Mikulski Archive for Space Telescopes (MAST). STScI is operated by the Association of Universities for Research in Astronomy, Inc., under NASA contract NAS5-26555. Also, we made use of the VizieR catalog access tool, CDS, Strasbourg, France.

ORCID iDs

R. Arun  <https://orcid.org/0000-0002-4999-2990>
 Blesson Mathew  <https://orcid.org/0000-0002-7254-191X>
 P. Manoj  <https://orcid.org/0000-0002-3530-304X>
 Mayank Narang  <https://orcid.org/0000-0002-0554-1151>

References

- Alecian, E., Wade, G. A., Catala, C., et al. 2013, *MNRAS*, **429**, 1001
 Alonso-Albi, T., Fuente, A., Bachiller, R., et al. 2009, *A&A*, **497**, 117
 Andre, P., Ward-Thompson, D., & Barsony, M. 1993, *ApJ*, **406**, 122
 Bailer-Jones, C. A. L., Rybizki, J., Fousneau, M., Mantelet, G., & Andrae, R. 2018, *AJ*, **156**, 58
 Baines, D., Oudmaijer, R. D., Porter, J. M., & Pozzo, M. 2006, *MNRAS*, **367**, 737
 Beltrán, M. T., & de Wit, W. J. 2016, *A&ARv*, **24**, 6
 Boehm, T., & Catala, C. 1995, *A&A*, **301**, 155
 Borges Fernandes, M., Kraus, M., Lorenz Martins, S., & de Araújo, F. X. 2007, *MNRAS*, **377**, 1343
 Bouvier, J., Alencar, S. H. P., Boutelier, T., et al. 2007, *A&A*, **463**, 1017
 Bressan, A., Marigo, P., Girardi, L., et al. 2012, *MNRAS*, **427**, 127
 Calvet, N., & Gullbring, E. 1998, *ApJ*, **509**, 802
 Chen, P. S., Shan, H. G., & Zhang, P. 2016, *NewA*, **44**, 1
 Choi, J., Dotter, A., Conroy, C., et al. 2016, *ApJ*, **823**, 102
 Costigan, G., Vink, J. S., Scholz, A., Ray, T., & Testi, L. 2014, *MNRAS*, **440**, 3444
 Cutri, et al. 2013, *yCat*, **2328**
 de Zeeuw, P. T., Hoogerwerf, R., de Bruijne, J. H. J., Brown, A. G. A., & Blaauw, A. 1999, *AJ*, **117**, 354
 Dotter, A. 2016, *ApJS*, **222**, 8
 ESA 1997, in ESA Special Publication 1200, The HIPPARCOS and TYCHO Catalogues. Astrometric and Photometric Star Catalogues Derived from the ESA HIPPARCOS Space Astrometry Mission (Noordwijk: ESA), *ESA SP-1200*
 Evans, D. W., Riello, M., De Angeli, F., et al. 2018, *A&A*, **616**, A4
 Fairlamb, J. R., Oudmaijer, R. D., Mendigutía, I., Ilee, J. D., & van den Ancker, M. E. 2015, *MNRAS*, **453**, 976
 Fairlamb, J. R., Oudmaijer, R. D., Mendigutía, I., Ilee, J. D., & van den Ancker, M. E. 2017, *MNRAS*, **464**, 4721
 Fedele, D., van den Ancker, M. E., Henning, T., Jayawardhana, R., & Oliveira, J. M. 2010, *A&A*, **510**, A72
 Fresneau, A., & Osborn, W. H. 2009, *A&A*, **503**, 1023
 Gaia Collaboration, Babusiaux, C., van Leeuwen, F., et al. 2018a, *A&A*, **616**, A10
 Gaia Collaboration, Brown, A. G. A., Vallenari, A., et al. 2018b, *A&A*, **616**, A1
 Gaia Collaboration, Brown, A. G. A., Vallenari, A., et al. 2016a, *A&A*, **595**, A2
 Gaia Collaboration, Prusti, T., de Bruijne, J. H. J., et al. 2016b, *A&A*, **595**, A1
 Getman, K. V., Feigelson, E. D., Broos, P. S., Micela, G., & Garmire, G. P. 2008, *ApJ*, **688**, 418
 Girard, T. M., van Altena, W. F., Zacharias, N., et al. 2011, *AJ*, **142**, 15
 Gorti, U., & Bhatt, H. C. 1993, *A&A*, **270**, 426
 Greene, T. P., Wilking, B. A., Andre, P., Young, E. T., & Lada, C. J. 1994, *ApJ*, **434**, 614
 Gullbring, E., Hartmann, L., Briceño, C., & Calvet, N. 1998, *ApJ*, **492**, 323
 Hamann, F., & Persson, S. E. 1992, *ApJS*, **82**, 285
 Hartmann, L., Calvet, N., Gullbring, E., & D'Alessio, P. 1998, *ApJ*, **495**, 385
 Henden, A. A., Templeton, M., Terrell, D., et al. 2016, *yCat*, **2336**
 Herbig, G. H. 1960, *ApJS*, **4**, 337
 Herbst, W., & Shevchenko, V. S. 1999, *AJ*, **118**, 1043
 Hernández, J., Calvet, N., Briceño, C., Hartmann, L., & Berlind, P. 2004, *AJ*, **127**, 1682
 Hillenbrand, L. A., Strom, S. E., Vrba, F. J., & Keene, J. 1992, *ApJ*, **397**, 613
 Høg, E., Fabricius, C., Makarov, V. V., et al. 2000, *A&A*, **355**, L27
 Jordi, C., Gebran, M., Carrasco, J. M., et al. 2010, *A&A*, **523**, A48
 Lada, C. J. 1987, in IAU Symp. 115, Star-forming Regions, ed. M. Peimbert & J. Jugaku (Dordrecht: Reidel), **1**
 Lada, C. J., & Wilking, B. A. 1984, *ApJ*, **287**, 610
 Luri, X., Brown, A. G. A., Sarro, L. M., et al. 2018, *A&A*, **616**, A9
 Malfait, K., Bogaert, E., & Waelkens, C. 1998, *A&A*, **331**, 211
 Manoj, P., Bhatt, H. C., Maheswar, G., & Muneer, S. 2006, *ApJ*, **653**, 657
 Mathew, B., Manoj, P., Narang, M., et al. 2018, *ApJ*, **857**, 30
 McClure, M. 2009, *ApJL*, **693**, L81
 Mendigutía, I., Calvet, N., Montesinos, B., et al. 2011a, *A&A*, **535**, A99
 Mendigutía, I., Eiroa, C., Montesinos, B., et al. 2011b, *A&A*, **529**, A34
 Mendigutía, I., Mora, A., Montesinos, B., et al. 2012, *A&A*, **543**, A59
 Mendigutía, I., Oudmaijer, R. D., Rigliaco, E., et al. 2015, *MNRAS*, **452**, 2837
 Muzerolle, J., D'Alessio, P., Calvet, N., & Hartmann, L. 2004, *ApJ*, **617**, 406
 Muzerolle, J., Hillenbrand, L., Calvet, N., Briceño, C., & Hartmann, L. 2003, *ApJ*, **592**, 266
 Muzerolle, J., Luhman, K. L., Briceño, C., Hartmann, L., & Calvet, N. 2005, *ApJ*, **625**, 906
 Natta, A., Testi, L., & Randich, S. 2006, *A&A*, **452**, 245
 Oudmaijer, R. D., Ababakr, K. M., & Fairlamb, J. R. 2017, *MmSAI*, **88**, 605
 Pecaut, M. J., & Mamajek, E. E. 2013, *ApJS*, **208**, 9
 Shu, F., Najita, J., Ostriker, E., et al. 1994, *ApJ*, **429**, 781
 Skrutskie, M. F., Cutri, R. M., Stiening, R., et al. 2006, *AJ*, **131**, 1163
 Takagi, Y., Itoh, Y., & Oasa, Y. 2014, *PASJ*, **66**, 88
 The, P. S., de Winter, D., & Perez, M. R. 1994, *A&AS*, **104**, 315
 van den Ancker, M. E., de Winter, D., & Tjin A Djie, H. R. E. 1998, *A&A*, **330**, 145
 Vieira, R. G., Gregorio-Hetem, J., Hetem, A., Stasińska, G., & Szczerba, R. 2011, *A&A*, **526**, A24
 Vieira, S. L. A., Corradi, W. J. B., Alencar, S. H. P., et al. 2003, *AJ*, **126**, 2971
 Vink, J. S., Drew, J. E., Harries, T. J., & Oudmaijer, R. D. 2002, *MNRAS*, **337**, 356
 Vioque, M., Oudmaijer, R. D., Baines, D., Mendigutía, I., & Pérez-Martínez, R. 2018, *A&A*, **620**, A128
 Waters, L. B. F. M., & Waelkens, C. 1998, *ARA&A*, **36**, 233
 Wilking, B. A. 1989, *PASP*, **101**, 229